C. R. Chimie 22 (2019) 838–843

Contents lists available at ScienceDirect

Comptes Rendus Chimie

www.sciencedirect.com

Full paper/Mémoire

Highly stable Pt/ITO catalyst as a promising electrocatalyst for direct methanol fuel cells

Van Thi Thanh Ho [a, *], Hau Quoc Pham [b], Thy Ho Thi Anh [c], At Van Nguyen [b], Khuong Anh Nguyen Quoc [a], Hau Thi Hien Vo [a], Thi Thuong Nguyen [d]

[a] Hochiminh City University of Natural Resources and Environment (HCMUMRE), Viet Nam
[b] Ho Chi Minh City University of Technology (HCMUT), VNU-HCM, Viet Nam
[c] Posco-Vietnam Ltd., Co, Viet Nam
[d] Center of Excellence for Functional Polymers and NanoEngineering, Nguyen Tat Thanh University, Ho Chi Minh City, Viet Nam

ARTICLE INFO

Article history:
Received 28 May 2019
Accepted 19 August 2019
Available online 20 September 2019

Keywords:
Tin-doped indium oxide
ITO
Pt/ITO
DMFC

ABSTRACT

Direct methanol fuel cells (DMFCs) have attracted considerable scientific interest because of their ease of operation and implementation; however, poor electrocatalytic activity and durability are the main hindrances for their commercial feasibility. Moreover, the deactivation of active Pt sites, due to the coverage of CO-like species during the electrochemical oxidation reaction, significantly degrades the electrochemical surface area (ECSA). In the present work, stable Pt-supported tin-modified indium oxide (ITO) was synthesized as a promising electrocatalyst towards the methanol oxidation reaction (MOR) in DMFCs. It was found that 20 wt% Pt/ITO yielded much higher current density (~0.71 mA/cm^2) than the state-of-the-art carbon-supported Pt (E-TEK) electrocatalyst. Furthermore, the I_f/I_b ratio, which featured the CO tolerance of the electrocatalyst, of 20 wt% Pt/ITO was found to be ~1.42, which is ~1.5-fold higher than that of 20 wt% Pt/C (E-TEK). Chronoamperometry results indicated that 20 wt% Pt/ITO manifested much higher stability than 20 wt% Pt/C (E-TEK).

1. Introduction

The development of green power sources to solve the negative consequences of fossil fuels remains the main challenge for researchers in the 21st century. Direct methanol fuel cells (DMFCs) have attracted tremendous attention because of their ease of operation and implementation; however, the poor electrocatalytic activity and durability of electrocatalysts are the main barriers for their large-scale commercialization [1,2]. Moreover, the deactivation of active Pt sites results in the significant degradation of their electrochemical surface area (ECSA) [3]. In addition, the most commonly used Pt/C electrocatalyst manifests several restrictions including the corrosion of the carbon support and the intrinsic weak interactions between the carbon support and Pt nanocatalyst, which consequently degrades the operating life of DMFCs [2–4]. To overcome these drawbacks, numerous efforts have been undertaken to develop robust supports with high corrosion tolerance and strong interactivity with noble metals, such as metal oxides [5–8] and metal-doped metal oxides [3,9,10].

Tin dioxide (SnO_2) possesses a superior ability to inhibit Pt-oxide elements at high potentials [11,12]. However, low electronic conductivity [13] and poor stability [12] are the major limitations for SnO_2 to be applied as supporting material in DMFCs. To circumvent these problems, Sn is generally incorporated into host lattices of materials that have low electrical resistance and excellent electrochemical

* Corresponding author.
E-mail address: httvan@hcmunre.edu.vn (V.T.T. Ho).

https://doi.org/10.1016/j.crci.2019.08.003
1631-0748/

stability [12,13]. According to Liu and Mustain [12], tin-doped indium oxide (ITO) manifests outstanding durability towards oxygen reduction reactivity (ORR). ITO exploits the strong interactions between Pt and Sn as well as the stability of indium oxide to deal with the major technical drawbacks of Pt/C catalyst (such as Pt sintering, dissolution and corrosion) [4,14].

Very few studies have reported the electrochemical activity of Pt/ITO electrocatalyst towards methanol electrooxidation reactions (MORs) in DMFCs. In the present work, Pt-supported ITO nanoparticles were successfully prepared through a modified chemical reduction route at room temperature. Moreover, the electrochemical measurements were carried out in acidic and methanol mediums to record the electrochemical activity and stability of 20 wt% Pt/ITO towards MOR. These experimental results indicated that the 20 wt% Pt/ITO exhibited higher activity and greater CO tolerance than the state-of-the-art carbon-supported Pt (E-TEK) electrocatalyst. In addition, the ITO exhibits a superior improvement in terms of reducing degradation rates in comparison with common commercial Pt nanoparticles anchored on a carbon support. These recommend that Pt/ITO have great potential to be used as an electrocatalyst for DMFCs.

2. Experimental procedure

2.1. Chemicals

Indium acetylacetonate [In (acac)$_3$, 99%] and oleylamine (70%) were obtained from ACROSS organics, Belgium. Tin (IV) bis (acetylacetonate) dichloride (98%), dihydrogen hexachloroplatinate (IV) hexahydrate ($H_2PtCl_6 \cdot 6H_2O$, 99.9%), Nafion 117 solution (~5% in a mixture of alcohol and water) and methanol (CH_3OH, 99.8%) were purchased from Sigma-Aldrich, USA. Sodium hydroxide (NaOH, 99%) and ethanol (99.7%) were procured from Xilong, China. Ethylene glycol (EG, 99.5%) was purchased from Fischer, USA.

2.2. Synthesis of ITO nanostructures

ITO nanostructures were prepared by a facile solgel process followed by mild calcination [12,15]. A mixture of 0.2699 g In (acac)$_3$ and 0.026 g Sn (acac)$_2Cl_2$ was first dissolved in 4 mL of oleylamine in a three-neck flask connected with a condenser. The reaction was then vigorously stirred at 235 °C for 3 h to form a dark yellow suspension. The as-obtained suspension was separated by centrifugation and washed with purified water until the supernatant became neutral to remove unreacted reagents and residual oleylamine. The as-prepared solid was dried overnight at 80 °C in the air to form a grey powder and subsequently calcined in a furnace for 3 h at three different temperatures of 400 °C, 500 °C and 600 °C. ITO samples obtained at 400 °C, 500 °C and 600 °C were denoted as ITO400, ITO500 and ITO600, respectively (Scheme 1).

2.3. Synthesis of 20 wt% Pt/ITO catalyst

The catalyst was synthesized by a modified chemical reduction method. A mixture of 3 mL of H_2PtCl_6 (0.05 M) and 0.5 mL of EG was first ultrasonicated for 20 min at 20 °C. ITO powder (46.8 mg) was then added into the mixture, and the pH of the as-obtained suspension was adjusted to 11 by NaOH solution. $NaBH_4$ (acted as a reducing agent) was then added dropwise into the suspension, and the mixture was vigorously stirred for 2 h at 60 °C. The as-obtained suspension was centrifuged and washed with purified water. Finally, the as-obtained product was dried overnight for further analysis (Scheme 2).

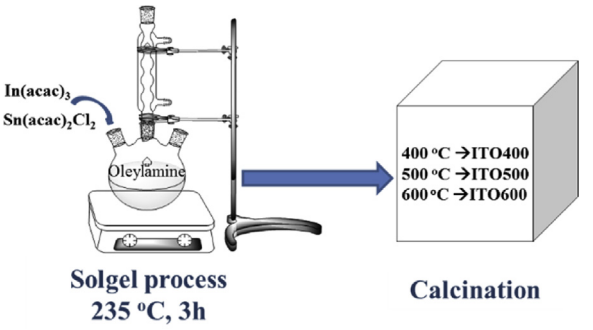

Scheme 1. Synthesis of tin-doped indium oxide.

2.4. Material characterization

The phase structures of the as-obtained samples were revealed by X-ray diffraction analysis (XRD; D2 PHASER-Brucker, Germany) in the 2θ range of 20°–80°. The morphologies and particle sizes of the samples were detected by transmission electron microscopy (TEM; JOEL-JEM 1400). For electrical conductivity measurement tests, pellets of diameter 10 mm and thickness 1 mm were made from dry samples using a hydraulic press under a pressure of 300 MPa and then dried overnight at 105 °C.

Electrochemical measurement tests were carried out in an EC-LAB electrochemistry device equipped with a silver/silver chloride (saturated KCl) reference electrode, a Pt counter electrode and a glassy carbon electrode (diameter of 5 mm). The catalyst ink was prepared through the following process: the catalyst powder was first ultrasonicated for 30 min in a solution consisting of ethanol and 0.5% Nafion. The surface of the glassy carbon disk was polished with 0.5-μm Al_2O_3 polishing powder (BAS) and then washed with ethanol and purified water. In the present work, all electrochemical potentials were described against the normal hydrogen electrode (NHE) scale. The catalyst electrode was activated by 100 cycles at a sweep rate of 50 mV/s. To measure the ECSA of the as-obtained catalyst, the electrochemical test was executed in nitrogen-saturated 0.5 M H_2SO_4 solution at a sweep rate of 50 mV/s. The electrocatalytic activity of the catalyst towards MOR was recorded in a solution of nitrogen-saturated 10 v/v% CH_3OH and 0.5 M H_2SO_4 at a scan rate of 50 mV/s. The chronoamperometry test was carried out in a methanol acidic media for 1000 s at an immobilized potential of 1.0 V to measure the poisoning resistance of the as-synthesized catalyst to intermediate carbonaceous species during MOR.

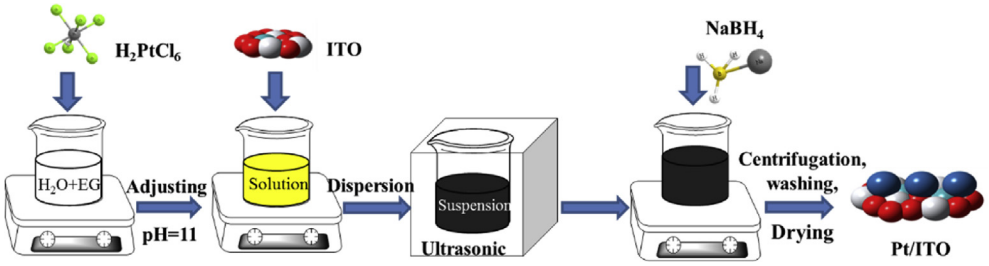

Scheme 2. Synthetic procedure for Pt/ITO catalyst. EG, ethylene glycol; ITO, tin-doped indium oxide.

3. Results and discussion

Fig. 1 displays the XRD patterns of ITO samples (ITO400, ITO500 and ITO600), SnO_2 (JCPDS 41–1445) and InO_3 (JCPDS 06–0416). All ITO samples possessed the cubic bixbyite structure of indium oxide, and the peaks at 2θ ~30.6°, 35.5°, 51° and 60.7° appeared from the (222), (400), (440) and (622) planes, respectively. Furthermore, no prominent SnO_2 peak was observed; it indicates that Sn was completely distributed into InO_3 lattices without forming any composite oxide after calcination. ITO400, due to its low calcination temperature, generated much lower XRD peak intensity than ITO500 and ITO600. The crystallite sizes of ITO400, ITO500 and ITO600 were measured by Scherrer equation [16,17] as ~9.25 nm, ~14.59 nm, and ~20.53 nm, respectively.

It is already proved that calcination plays an important role in preventing particle agglomeration [1]. The TEM morphologies of three different ITO samples after calcination are exhibited in Fig. 2. ITO400 was composed of nanoflower-shaped clusters and discrete spherical particles with an average size of 10 nm. When the calcination temperature reached 500 °C, uniform grains of diameters 15–20 nm were noticed in the morphology. However, the microstructure of ITO600 consisted of large spherical nanoparticles of diameter 30 nm. These results could be understood by the influences of calcination on removing organic ligand–encapsulated particle surfaces to form distinct particles at over 500 °C in an oxygen-rich environment. Beyond 500 °C, ITO particles generally have a high tendency to form larger particles. Hence, the surface areas of ITO samples decreased dramatically with the increasing calcination temperature (109.153 m^2/g, 72.533 m^2/g and 42.333 m^2/g for ITO400, ITO500 and ITO600, respectively). Moreover, the pore volume and the pore size of ITO400 were measured to be 0.071 cc/g and 1.18 nm, respectively; however, these values for ITO500 and ITO600 could not be determined, which could be explained for their much smaller surface areas than ITO400 [1].

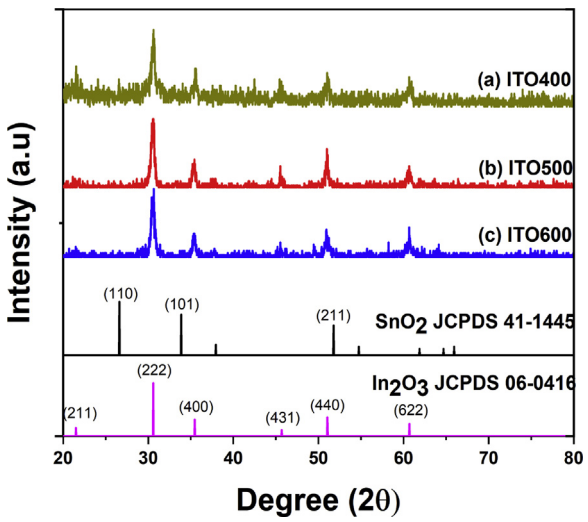

Fig. 1. XRD patterns of ITO samples. (a) ITO400; (b) ITO500; (c) ITO600. ITO, tin-doped indium oxide; XRD, X-ray diffraction analysis.

The electrical conductivity values of ITO samples were measured by the four-point probe technique, and the corresponding results are presented in Fig. 3. The electrical conductivity values of all ITO samples were found to be profoundly higher than those of commercial SnO_2 (10^{-6} S/cm) [1,12], Sb-doped SnO_2 (0.11 S/cm) [9], Ru-doped SnO_2 ($2.5 \cdot 10^{-3}$ S/cm) [18], and $Ti_{0.7}Mo_{0.3}O_2$ ($2.8 \cdot 10^{-4}$ S/cm) [4], and the highest conductivity of 2.60 S/cm was obtained for ITO600. The variation in electrical conductivity of the samples could be attributed to the rise in their intrinsic charge carriers during calcination. In addition, calcination also contributed to the formation of highly crystalline structures.

The XRD patterns of 20 wt% Pt/ITO electrocatalysts are demonstrated in Fig. 4 (a). After the reduction process, the XRD profiles of 20 wt% Pt/ITO samples remained well consistent with original ITO patterns, thus indicating the stability of ITO nanostructures. Moreover, three Pt peaks at 2θ ~39°, 46° and 68° appeared corresponding with (111), (200) and (220) Pt planes, respectively, (JCPDS 01–1194). It is worth noting that all diffraction peaks of Pt were broadened because of the small diameter of deposited Pt nanoform. The structural properties (surface area, particle size and electrochemical surface area) of 20 wt% Pt/ITO at different calcination temperatures are depicted in Table 1.

The ECSA values of three different 20 wt% Pt/ITO samples and the commercial carbon-supported Pt (E-TEK) electrocatalyst were compared (Fig. 5). The ECSA of these catalysts was estimated based on hydrogen adsorption (Q_H) and then divided into electric charge transfer of hydrogen adsorption (210 μC/cm). The ECSA value of 20 wt% Pt/ITO400 (44.1 m^2/gPt) was found to be smaller than those of other catalysts, and it can be attributed to the agglomerated morphology of ITO400. However, the ECSA value of 20 wt%

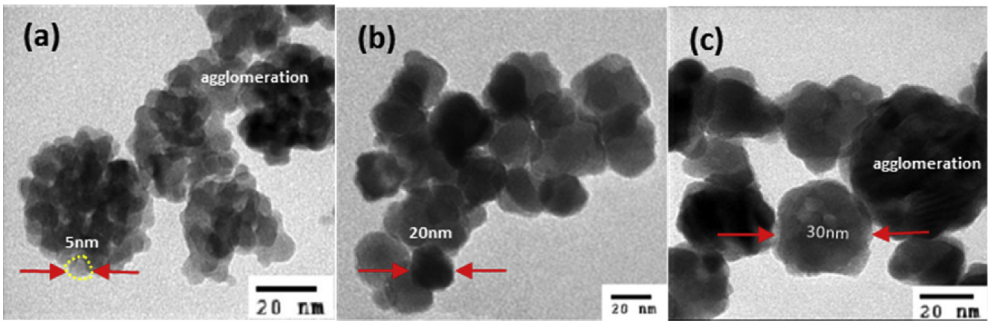

Fig. 2. TEM images of (a) ITO400; (b) ITO500; (c) ITO600. ITO, tin-doped indium oxide; TEM, transmission electron microscopy.

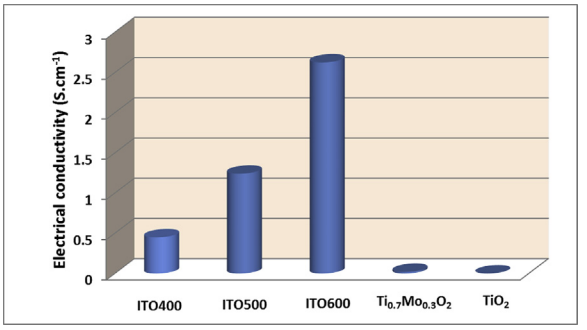

Fig. 3. The comparison of electrical conductivity of ITO samples with various calcination temperatures and other ITO and noncarbon supports. ITO, tin-doped indium oxide.

Pt/ITO600 was approximately equal to that of 20 wt% Pt/C (~64.6 m^2/gPt). The 20 wt% Pt/ITO600 catalyst yielded the highest ECSA value because of the higher electrical conductivity of ITO600 than those of ITO400 and ITO500 (Fig. 3), thereby facilitating efficient electron conduction during electrochemical reactions [19,20].

Table 1
Properties of the 20 wt% Pt/ITO electrocatalyst.

Catalyst	S_{BET} of ITO (m^2/g)	Particle size of Pt (nm)	ECSA (m^2/g)
20 wt% Pt/ITO400	109.2	~10.0	44.1
20 wt% Pt/ITO500	72.5	~9.9	54.5
20 wt% Pt/ITO600	42.3	~8.9	63.4

ECSA, electrochemical surface area; ITO, tin-doped indium oxide.

The cyclic voltammogram of Pt/C exhibited a major peak at 1.2 V (Fig. 5); it indicates that the oxidation of carbon significantly deteriorated the catalyst. However, no oxidation peaks for 20 wt% Pt/ITO samples were noticed within the selected cyclic voltammetry (CV) range, thus suggesting the formation of stable ITO supports.

To reveal the catalytic and CO tolerance properties of 20 wt% Pt/ITO samples during MOR, cyclic voltammograms were recorded in a solution of nitrogen-saturated 10 v/v% CH_3OH and 0.5 M H_2SO_4 at a scan rate of 50 mV/s (Fig. 6). All CV profiles consisted of two major peaks (appeared from the oxidation of methanol and residual intermediates) during the forward and upward scans. The CO-poisoning

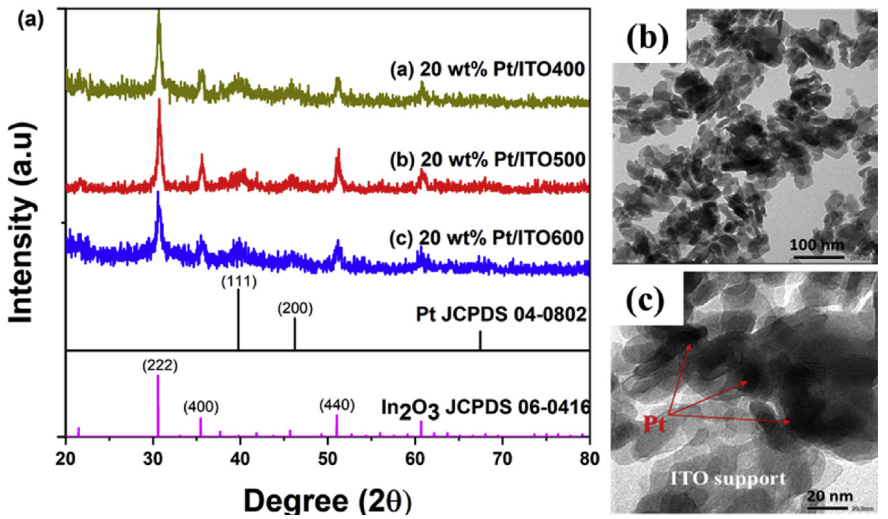

Fig. 4. XRD patterns of (a) 20 wt% Pt/ITO400; 20 wt% Pt/ITO500; and 20 wt% Pt/ITO600 and (b, c) 20 wt% Pt/ITO500 with different scale bar. ITO, tin-doped indium oxide; XRD, X-ray diffraction analysis.

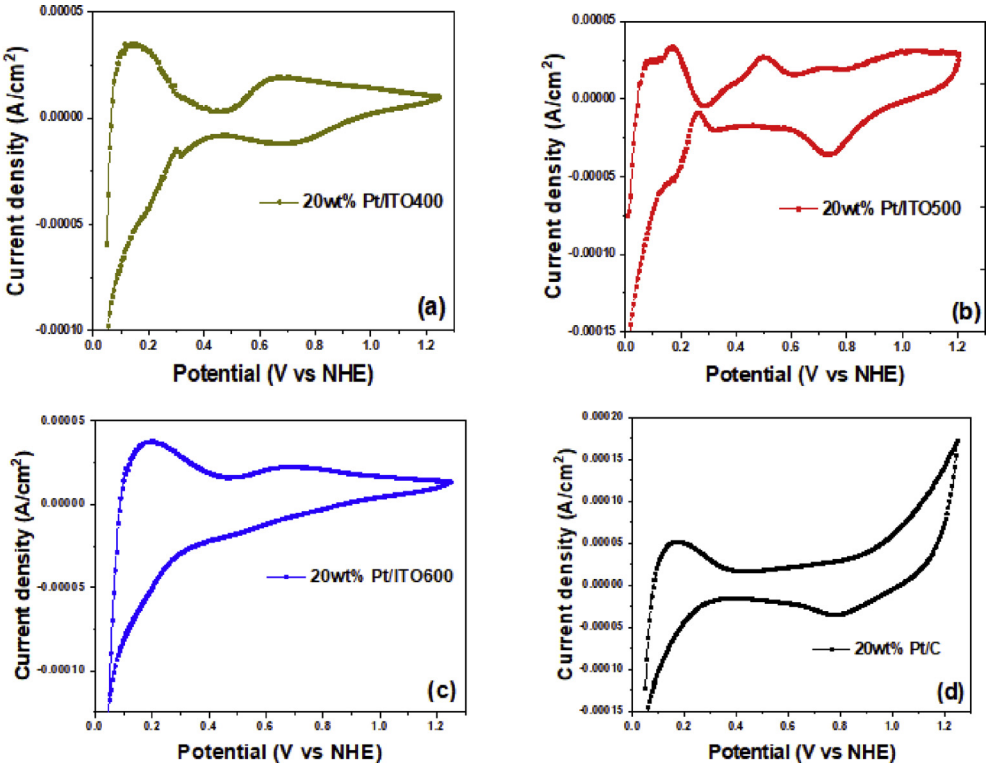

Fig. 5. Cyclic voltammetry profiles for (a) 20 wt% Pt/ITO400, (b) 20 wt% Pt/ITO500, (c) 20 wt% Pt/ITO600 and (d) Pt/C in acidic media. ITO, tin-doped indium oxide; NHE, normal hydrogen electrode.

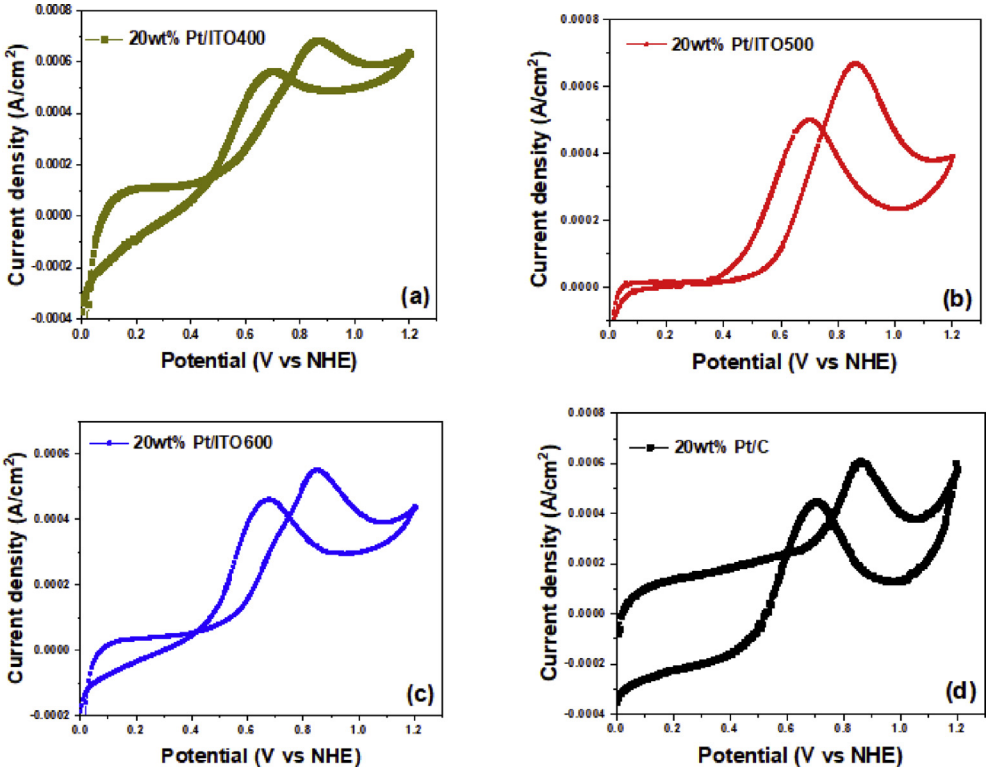

Fig. 6. Cyclic voltammograms for methanol oxidation reaction of (a) 20 wt% Pt/ITO400, (b) 20 wt% Pt/ITO500, (c) 20 wt% Pt/ITO600 and (d) 20 wt% Pt/C. ITO, tin-doped indium oxide; NHE, normal hydrogen electrode.

Table 2
Electrochemical parameters of Pt/ITO for the methanol oxidation reaction.

Catalyst	S_{ESA-H} (m^2/g Pt)	I_f (mA)	I_b (mA)	I_f/I_b
20 wt% Pt/ITO400	44.1	0.68	0.56	1.24
20 wt% Pt/ITO500	54.5	0.71	0.50	1.42
20 wt% Pt/ITO600	63.4	0.56	0.46	1.20
20 wt% Pt/C	64.6	0.60	0.49	1.22

ITO, tin-doped indium oxide.

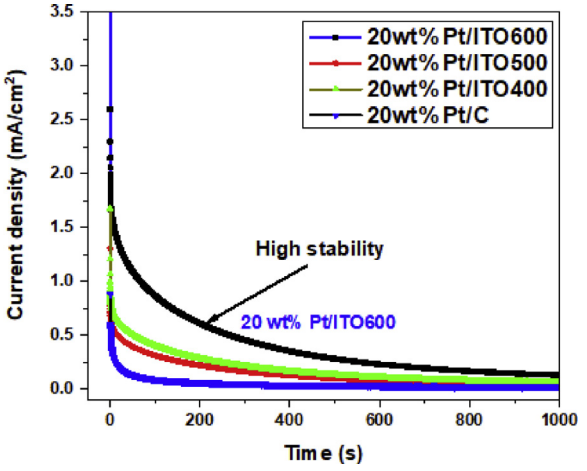

Fig. 7. Chronoamperometry analyses of the Pt/ITO catalysts at 1.0 V in 1 M CH_3OH/0.5 M H_2SO_4 solution. ITO, tin-doped indium oxide.

factor is associated with the ratio of currents in the forward and backward scans (I_f/I_b). A small I_f/I_b ratio implies the elimination of residual carbonaceous intermediates (mostly CO species) during the forward scan, thus resulting in higher CO tolerance [21–23]. The 20 wt% Pt/ITO500 catalyst yielded the highest CO tolerance because of its highest I_f/I_b ratio of ~1.42, whereas other two catalysts led to the same I_f/I_b value of ~1.22 (Table 2). The promising CO tolerance of 20 wt% Pt/ITO500 can be ascribed to the strong affinity between Pt and ITO500 [12], which is not normally found in the Pt/C catalyst [4,24,25].

The stability of Pt/ITO catalysts was investigated by chronoamperometry (Fig. 7). In the beginning, the current densities of 20 wt% Pt/ITO catalysts declined rapidly because of the absorption of poisoning intermediates. The 20 wt% Pt/C catalyst represented a rapid degradation only after 100 s; however, all 20 wt% Pt/ITO samples manifested much slower degradation rates. The 20 wt% Pt/ITO600 catalyst had the slowest degradation rate, thus suggesting its high tolerance against poisoning species. The high CO tolerance of 20 wt% Pt/ITO samples can be attributed to the strong electron affinity between Pt and ITO substrates that suppress the adhesion of CO species on Pt active surfaces.

4. Conclusion

ITO electrocatalysts were successfully prepared through a facile solgel route followed by calcination, and the effects of calcination temperature on ITO morphologies were investigated. The ITO sample calcined at 500 °C caused less particle agglomeration than the sample calcined at 400 °C, and it can be attributed to the removal of organic ligands after calcination at 500 °C. Moreover, the ITO catalyst calcined at 600 °C led to particle growth and had the smallest surface area. More importantly, ITO showed high electrical conductivity that could be applied as a good support material in fuel cells. The results of electrochemical analyses indicated that the ECSA values of Pt/ITO and Pt/C catalysts were almost the same. However, Pt/ITO catalysts exhibited much better MOR electrocatalytic activity, CO tolerance and durability than commercial Pt/C.

Acknowledgements

The research has received financial support by the National Foundation for Science and Technology Development (NAFOSTED) given under a special program for Basic Research Projects in Natural Science 140 2014 (grant No. 104.03–2014.92).

References

[1] A.K.Q. Nguyen, T.T. Huynh, V.T.T. Ho, Mol. Cryst. Liq. Cryst. 635 (2016) 32–39.
[2] Z. Yavari, M. Noroozifar, M. Khorasani-Motlagh, J. Exp. Nanosci. 11 (2016) 798–815.
[3] V.T.T. Ho, N.G. Nguyen, C.-J. Pan, J.-H. Cheng, J. Rick, W.-N. Su, et al., Nano Energy 1 (2012) 687–695.
[4] V.T. Ho, C.J. Pan, J. Rick, W.N. Su, B.J. Hwang, J. Am. Chem. Soc. 133 (2011) 11716–11724.
[5] P. Dhanasekaran, S. Vinod Selvaganesh, L. Sarathi, D. Santoshkumar, Bhat. Electrocatalysis 7 (2016) 495–506.
[6] H.N. Nong, H.-S. Oh, T. Reier, E. Willinger, M.-G. Willinger, Valeri PetkovAngew Chem Int Ed Engl 54 (2015) 2975–2979.
[7] K.-W. Park, Y.-E. Sung, M.F. Toney, Electrochem. Commun. 8 (2006) 359–363.
[8] S.T. Nguyen, J.-M. Lee, Y. Yang, X. Wang, Ind. Eng. Chem. Res. 51 (2012) 9966–9972.
[9] K.-S. Lee, I.-S. Park, Y.-H. Cho, D.-S. Jung, N. Jung, H.-Y. Park, et al., J. Catal. 258 (2008) 143–152.
[10] Y.-J. Wang, D.P. Wilkinson, V. Neburchilov, C. Song, A. Guest, J. Zhang, J. Mater. Chem. 2 (2014) 12681–12685.
[11] M. Nakada, A. Ishihara, S. Mitsushima, N. Kamiya, K. Ota, Electrochem. Solid State Lett. 10 (2007) F1–F4.
[12] Y. Liu, W.E. Mustain, J. Am. Chem. Soc. 135 (2013) 530–533.
[13] I. Saadeddin, B. Pecquenartd, J.P. Manaud, R. Decourt, C. Labrugere, T. Bufereau, B. Campet, Appl. Surf. Sci. 253 (2007) 5240–5249.
[14] Y. Shao, J. Liu, Y. Wanga, Y. Lin, J. Mater. Chem. 19 (2009) 46–59.
[15] K.A.N. Quoc, H.T.H. Vo, T.P. Dinh, L.G. Bach, V.T.T. Ho, J. Nanosci. Nanotechnol. 18 (2018) 7246–7250.
[16] A. Madhumitha, V. Preethi, S. Kanmani, Int. J. Hydrogen Energy 43 (2018) 3946–3956.
[17] S. Rajendran, T.K.A. Hoang, R. Boukherroub, D.E. Diaz-Droguett, F. Gracia, M.A. Gracia-Pinilla, et al., Int. J. Hydrogen Energy 43 (2018) 2861–2868.
[18] H.L. Pang, X.H. Zhang, X.X. Zhong, B. Liu, X.G. Wei, Y.F. Kuang, et al., J. Colloid Interface Sci. 319 (2008) 193–198.
[19] S. Samad, K.S. Loh, W.Y. Wong, T.K. Lee, Jaka Sunarso, S.T. Chong, et al., Int. J. Hydrogen Energy 43 (2018) 7823–7854.
[20] S.T. Nguyen, Y. Yang, X. Wang, Appl. Catal. B Environ. 113–114 (2012) 261.
[21] K. Mikkelsen, B. Cassidy, N. Hofstetter, L. Bergquist, A. Taylor, D.A. Rider, et al., Chem. Mater. 26 (2014) 6928–6940.
[22] K. Zhang, W. Yang, C. Ma, Y. Wang, C. Sun, Y. Chen, et al., NPG Asia Mater. 7 (2015) e153.
[23] H. Zhang, Y. Yin, Y. Hu, C. Li, P. Wu, S. Wei, et al., J. Phys. Chem. C 114 (2010) 11861–11867.
[24] L. Castanheira, L. Dubau, M. Mermoux, G. Berthomé, N. Caqué, E. Rossinot, et al., ACS Catal. 5 (2015) 2184–2194.
[25] S.-E. Jang, H. Kim, J. Am. Chem. Soc. 132 (2010) 14700–14701.